



OPEN ACCESS

EDITED BY

John Common,
Agency for Science, Technology and
Research (A*STAR), Singapore

REVIEWED BY

Yoshikazu Uchida,
Northern California Institute for Research
and Education (NCIRE), United States
Daria Chudakova,
Federal Biomedical Agency, Russia
Robert Rice,
University of California, Davis,
United States

*CORRESPONDENCE

Edel A. O'Toole,
✉ e.a.otoole@qmul.ac.uk

RECEIVED 28 February 2023

ACCEPTED 18 May 2023

PUBLISHED 07 June 2023

CITATION

McGeoghan F, Camera E, Maiellaro M,
Menon M, Huang M, Dewan P, Ziaj S,
Caley MP, Donaldson M, Enright AJ and
O'Toole EA (2023), RNA sequencing and
lipidomics uncovers novel
pathomechanisms in recessive X-
linked ichthyosis.
Front. Mol. Biosci. 10:1176802.
doi: 10.3389/fmolb.2023.1176802

COPYRIGHT

© 2023 McGeoghan, Camera, Maiellaro,
Menon, Huang, Dewan, Ziaj, Caley,
Donaldson, Enright and O'Toole. This is
an open-access article distributed under
the terms of the [Creative Commons
Attribution License \(CC BY\)](#). The use,
distribution or reproduction in other
forums is permitted, provided the original
author(s) and the copyright owner(s) are
credited and that the original publication
in this journal is cited, in accordance with
accepted academic practice. No use,
distribution or reproduction is permitted
which does not comply with these terms.

RNA sequencing and lipidomics uncovers novel pathomechanisms in recessive X-linked ichthyosis

Farrell McGeoghan¹, Emanuela Camera², Miriam Maiellaro²,
Manasi Menon¹, Mei Huang¹, Priya Dewan¹, Stela Ziaj³,
Matthew P. Caley¹, Michael Donaldson⁴, Anton J. Enright⁵ and
Edel A. O'Toole^{1,3*}

¹Centre for Cell Biology and Cutaneous Research, Blizard Institute, Faculty of Medicine and Dentistry, Queen Mary University of London, London, United Kingdom, ²Laboratory of Cutaneous Physiopathology, San Gallicano Dermatological Institute-IRCCS, Rome, Italy, ³Department of Dermatology, Royal London Hospital, Barts Health NHS Trust, London, United Kingdom, ⁴Senzo Health Limited, London, United Kingdom, ⁵Department of Pathology, University of Cambridge, Cambridge, United Kingdom

Recessive X-linked ichthyosis (RXLI), a genetic disorder caused by deletion or point mutations of the steroid sulfatase (*STS*) gene, is the second most common form of ichthyosis. It is a disorder of keratinocyte cholesterol sulfate retention and the mechanism of extracutaneous phenotypes such as corneal opacities and attention deficit hyperactivity disorder are poorly understood. To understand the pathomechanisms of RXLI, the transcriptome of differentiated primary keratinocytes with *STS* knockdown was sequenced. The results were validated in a stable knockdown model of *STS*, to confirm *STS* specificity, and in RXLI skin. The results show that there was significantly reduced expression of genes related to epidermal differentiation and lipid metabolism, including ceramide and sphingolipid synthesis. In addition, there was significant downregulation of aldehyde dehydrogenase family members and the oxytocin receptor which have been linked to corneal transparency and behavioural disorders respectively, both of which are extracutaneous phenotypes of RXLI. These data provide a greater understanding of the causative mechanisms of RXLI's cutaneous phenotype, and show that the keratinocyte transcriptome and lipidomics can give novel insights into the phenotype of patients with RXLI.

KEYWORDS

ichthyosis, skin barrier, steroid sulfatase, ceramides, lipidomics

Introduction

Recessive X-linked ichthyosis (RXLI) is a genetic disorder occurring in approximately 1:1500 males (Craig et al., 2010). The disease presents in the first year of life with scaling and erythema developing with time into brown polygonal scales most marked on the shins, neck and abdomen but generally sparing the palmoplantar skin and flexures. There are often extracutaneous features, which include asymptomatic corneal opacities, neurological features (autism-related traits and attention deficit hyperactivity disorder (ADHD)) and hypogonadism (Crane and Paller, 2022). In an Italian study, ADHD was reported in 9 out of 33 RXLI patients (Diociaiuti et al., 2019). A study of female carriers showed increased rates of autism-related traits and post-partum depression compared to controls (Cavenagh, Chatterjee, and Davies, 2019).

A recent study using UK Biobank identified an association with atrial arrhythmias, haemorrhage after surgery and palmar fascial fibromatosis (Brcic et al., 2020), (Brcic

et al., 2022). An online survey showed self-reported abnormal heart rhythms in 28%–35% of male and female carriers of Xp22.31 deletions and suggested that cardiac screening might be important (Wren et al., 2022).

The causative gene steroid sulfatase (STS) encodes a protein which hydrolyses cholesterol sulfate (CSO₄) to cholesterol (Koppe et al., 1978) (Tiepolo et al., 1980; Yen et al., 1987). In the epidermis this occurs in the upper granular layer and stratum corneum, where STS activity increases up to 20-fold compared to the basal layer (Williams et al., 1983). In RXLI there is a total loss of STS activity in all layers of the epidermis, leading to adverse effects on the lipid content, delayed desquamation and acanthosis which is thought to result from CSO₄ levels increasing up to 20-fold. In addition, mothers giving birth to babies with RXLI often experience prolonged labour (Paige et al., 1994).

Previous research *in vitro* has indicated CSO₄ can affect the activity and expression of transglutaminase (TGM) 1, a cross-linking enzyme important for the formation of the cornified envelope (CE) and the cornified lipid envelope (CLE) (Nemes et al., 2000). Analysis of RNA sequencing of human keratinocyte HaCaT cells treated with cholesterol and cholesterol sulfate identified increased Yippee-like 3 (YPEL3), a gene expected to affect keratinocyte differentiation. Increased expression of YPEL3 in STS-deficient cell lines promoted cellular senescence and increased involucrin and loricrin (Baek et al., 2021). In addition, CSO₄ has been shown *in vitro* to be a serine protease inhibitor, so it is theorised there is inhibition of kallikreins (KLK) 5 and 7 in RXLI, which would prevent desquamation (Sato et al., 1998). Thus far, these data have not been confirmed in RXLI samples and there is no data on the pathogenesis of extracutaneous signs, other than in those patients with contiguous deletions.

Here, we confirm reduced TGM1 expression and activity *in vivo* using RXLI skin samples and show upregulated expression of desmoglein-1 and reduced expression of KLK5. Furthermore, we report the results of transcriptome sequencing from primary keratinocytes with STS knockdown and validation in an STS knockdown model and RXLI skin. Immunostaining showed reduced epidermal expression of UDP-glucose ceramide glycosyltransferase (UGCG) and alkaline ceramidase 1 (ACER1), two important components of the ceramide synthesis pathway. Corneal opacities were linked to aldehyde dehydrogenase 1 family member A1 (ALDH1A1) and aldehyde dehydrogenase 3 family member A1 (ALDH3A1) downregulation, both of which are involved in corneal transparency (Lassen et al., 2007). A reduction was seen in oxytocin receptor (OXTR) expression which has been linked to behavioural disorders and prolonged labour (Fuchs et al., 1982) (Jacob et al., 2007). These data provide novel explanations for the development of extracutaneous features in RXLI, and further the understanding of how CSO₄ and STS interact and regulate epidermal differentiation and lipid synthesis.

Results

RNA sequencing in primary keratinocytes with siRNA knockdown of STS

We analysed a data set of triple biological replicates from primary keratinocytes with siRNA knockdown of STS. The data discussed in this

publication have been deposited in NCBI's Gene Expression Omnibus and are accessible through GEO Series accession number GSE232622 (Barrett et al., 2013). After applying a cut-off point of $p < 0.05$ there were 3,454 upregulated and 3,608 downregulated genes in the transcriptome data set. Genes with log-fold change >2 were inputted into the Gene Ontology GO Enrichment Analysis using the PANTHER Classification System to identify enriched biological processes. Table 1 shows the top 20 downregulated biological processes. Of interest, these included enrichment of genes involved in cholesterol efflux (4.9-fold), astrocyte development (4.55-fold), keratinization (4.22-fold), keratinocyte differentiation (3.7-fold) and cardiac septum morphogenesis (3.19-fold). Table 2 shows the top 20 upregulated biological processes. This included enrichment of genes involved in negative regulation of epithelial cell differentiation (6.2-fold), cell substrate junction assembly and organisation (5.53 and 5.39-fold, respectively) and response to oestrogen (4.22-fold).

Development of RXLI model and characterization of transglutaminase expression and desquamation

To validate genes of interest, skin biopsies were obtained from three RXLI patients. To confirm any changes observed were due to loss of STS, we also created using lentiviral particles STS shRNA knockdown (STS KD1 and STS KD2) and non-targeting control (NTC) cell lines in immortalised N/TERT keratinocytes. Knockdown was confirmed using qPCR showing greater KD in STS KD 2 (Supplementary Figure S1A). These cell lines were used to make a 3D model of RXLI (Supplementary Figure S1B). The 3D model of RXLI had decreased expression of TGM1 and decreased activity of TGM1 and TGM3 (pH 8.4) with a greater decrease in STS KD2 skin equivalents (Figure 1A). Decreased activity was also seen in the RXLI 3D model at pH 7.4 (Supplementary Figure S2), confirming that TGM1 activity alone was also reduced. In RXLI skin samples, there was a significant decrease of TGM1 expression and activity (Figures 1B, C). Desquamation requires a KLK cascade and CSO₄ has been previously shown to inhibit KLK5 and KLK7 (Sato et al., 1998). We confirmed reduction of KLK5 in RXLI skin. KLK5 self-activates and then begins to activate other kallikreins, potentially making it the most important kallikrein for desquamation (Caubet et al., 2004). A reduction of KLK5 expression as observed here would likely affect the rest of the cascade, resulting in a reduction of several kallikreins required for desquamation resulting in the delay of desquamation seen in RXLI. Interestingly, loss of STS increased desmoglein 1 (DSG1) expression (Log Fold Change 1.049) in the RNA sequencing data set. Cell adhesion proteins are targets of KLKs including DSG1, desmocollin 1 (DSC1) and corneodesmosin (CDSN). The increase in DSG1 was confirmed by immunostaining in both the RXLI model (more obvious in STS KD2) in Figure 1A and in RXLI skin (Figures 1B, C), consistent with the reduced desquamation observed.

Reduced expression of lipid metabolism enzymes in the RXLI model and skin

Differentially expressed genes in primary keratinocytes with STS knockdown included ACER1 and UGCG, which encode enzymes important for lipid metabolism in the epidermis (Amen et al., 2013) (Sun et al., 2008). Alkaline ceramidase 1 hydrolyses long-chain

TABLE 1 Gene Ontology annotation of biological processes downregulated in keratinocytes with siRNA knockdown of STS. FDR = False discovery rate. Expected = expected number of genes downregulated. Fold-enrichment- Actual number of genes downregulated/expected.

GO biological processes	Reference list	Downregulated (1292)	Expected	Fold-enrichment	Raw <i>p</i> -value	FDR
antigen processing and presentation of endogenous peptide antigen (GO:0002483)	19	8	1.19	6.71	1.17E-04	1.06E-02
response to interferon-alpha (GO:0035455)	23	8	1.44	5.54	3.36E-04	2.39E-02
neural tube patterning (GO:0021532)	33	11	2.07	5.31	3.67E-05	4.39E-03
positive regulation of cholesterol efflux (GO:0010875)	26	8	1.63	4.9	6.61E-04	3.95E-02
antigen processing and presentation of endogenous antigen (GO:0019883)	26	8	1.63	4.9	6.61E-04	3.94E-02
astrocyte development (GO:0014002)	35	10	2.2	4.55	2.38E-04	1.90E-02
keratinization (GO:0031424)	83	22	5.21	4.22	1.68E-07	6.44E-05
ventricular septum morphogenesis (GO:0060412)	41	10	2.57	3.89	6.90E-04	4.05E-02
keratinocyte differentiation (GO:0030216)	138	32	8.66	3.7	4.75E-09	3.39E-06
intermediate filament organization (GO:0045109)	70	16	4.39	3.64	3.81E-05	4.49E-03
negative regulation of viral genome replication (GO:0045071)	57	13	3.58	3.63	2.03E-04	1.66E-02
SMAD protein signal transduction (GO:0060395)	63	14	3.95	3.54	1.48E-04	1.31E-02
embryonic digit morphogenesis (GO:0042733)	59	13	3.7	3.51	2.71E-04	2.03E-02
roof of mouth development (GO:0060021)	92	20	5.77	3.46	8.17E-06	1.41E-03
aorta development (GO:0035904)	56	12	3.51	3.41	5.73E-04	3.54E-02
epidermal cell differentiation (GO:0009913)	201	42	12.61	3.33	3.18E-10	2.94E-07
BMP signaling pathway (GO:0030509)	91	19	5.71	3.33	2.23E-05	3.09E-03
cardiac septum morphogenesis (GO:0060411)	70	14	4.39	3.19	3.80E-04	2.61E-02
intermediate filament cytoskeleton organization (GO:0045104)	92	18	5.77	3.12	7.58E-05	7.62E-03
intermediate filament-based process (GO:0045103)	93	18	5.84	3.08	8.56E-05	8.28E-03

ceramides to sphingosine, which is then phosphorylated to form sphingosine-1-phosphate, regulated by sphingosine 1 kinase (SPHK1). The UGCG enzyme catalyses the first step of glycosphingolipid production, synthesising glucosylceramides (GluCers) from ceramides and UDP-glucose. Loss of these enzymes could affect bioactive lipid content within the epidermis, so RXLI skin samples and the 3D model were immunostained for ACER1 and UGCG (Figures 2A, B). In the 3D model, expression of all 3 proteins was reduced in both STS KD models (Figure 2A). As previously shown, ACER1 was expressed in differentiated epidermis with a clear reduction in RXLI skin (see Figures 2B, C). The UGCG expression was strong in normal basal epidermis with weaker expression in the upper epidermis and was markedly decreased in

RXLI skin (see Figures 2B, C). Expression of SPHK1 was seen throughout the epidermis in both the NTC 3D model and in normal control skin. A reduction was seen in both STS KD models and in RXLI epidermis (see Figures 2A–C).

Reduced expression of aldehyde dehydrogenases and the oxytocin receptor in the RXLI model and skin

The transcriptome of primary keratinocytes with STS knockdown showed altered expression of *ALDH1A1*, *ALDH3A1* and *OXTR*. Investigation of the literature indicated

TABLE 2 Gene Ontology annotation of biological processes upregulated in keratinocytes with siRNA knockdown of STS. FDR = False discovery rate.

GO biological processes	Reference list	Upregulated (745)	Expected	Fold-enrichment	Raw p-value	FDR
endoderm formation (GO:0001706)	54	13	1.95	6.65	4.61E-07	3.28E-04
endodermal cell differentiation (GO:0035987)	44	10	1.59	6.28	1.51E-05	3.70E-03
negative regulation of epithelial cell differentiation (GO:0030857)	49	11	1.77	6.2	6.29E-06	1.97E-03
regulation of cell migration involved in sprouting angiogenesis (GO:0090049)	38	8	1.38	5.82	1.71E-04	2.34E-02
regulation of transforming growth factor beta production (GO:0071634)	39	8	1.41	5.67	2.00E-04	2.64E-02
cell-substrate junction assembly (GO:0007044)	40	8	1.45	5.53	2.33E-04	2.97E-02
regulation of blood coagulation (GO:0030193)	70	14	2.53	5.53	1.17E-06	5.56E-04
negative regulation of blood coagulation (GO:0030195)	46	9	1.66	5.41	1.11E-04	1.70E-02
cell-substrate junction organization (GO:0150115)	41	8	1.48	5.39	2.70E-04	3.36E-02
regulation of hemostasis (GO:1900046)	72	14	2.61	5.37	1.57E-06	6.84E-04
negative regulation of hemostasis (GO:1900047)	47	9	1.7	5.29	1.28E-04	1.86E-02
regulation of coagulation (GO:0050818)	75	14	2.71	5.16	2.40E-06	9.40E-04
negative regulation of coagulation (GO:0050819)	50	9	1.81	4.97	1.93E-04	2.62E-02
positive regulation of blood vessel endothelial cell migration (GO:0043536)	54	9	1.95	4.61	3.22E-04	3.88E-02
regulation of wound healing (GO:0061041)	130	21	4.7	4.46	7.01E-08	8.45E-05
endoderm development (GO:0007492)	81	13	2.93	4.44	2.30E-05	5.08E-03
response to estrogen (GO:0043627)	72	11	2.61	4.22	1.43E-04	1.99E-02
negative regulation of wound healing (GO:0061045)	69	10	2.5	4.01	4.15E-04	4.72E-02
positive regulation of smooth muscle cell proliferation (GO:0048661)	85	12	3.08	3.9	1.42E-04	1.98E-02
regulation of ERBB signaling pathway (GO:1901184)	78	11	2.82	3.9	2.68E-04	3.36E-02

they could be linked to extracutaneous features of RXLI. There is evidence that ALDH1A1 and ALDH3A1 are important for transparency of the cornea (Lassen et al., 2007; Arrowsmith and Wray, 2014), whereas OXTR has been linked to behavioural disorders and is known to regulate parturition (Rijlaarsdam et al., 2017) (Arrowsmith and Wray, 2014). Thus, immunostaining for ALDH1A1, ALDH3A1 and OXTR was performed in the RXLI model (Figure 3A), while the expression of ALDH1A1, ALDH3A1 and OXTR was also investigated in normal control skin and RXLI skin (Figure 3B). All three had decreased expression in the RXLI model compared to NTC (Figure 3A). ALDH1A1 was expressed in the stratum corneum and basal epidermis close to the basement membrane in control skin and markedly reduced

expression was observed in RXLI skin (Figures 3B, C). ALDH3A1 was expressed in suprabasal epidermis in normal skin and was markedly reduced in RXLI skin. OXTR expression was present in the basal epidermis in normal skin and was markedly decreased in RXLI skin (Figure 3B).

Lipidomic analysis of the RXLI model

In order to understand the effect of STS knockdown further, changes in lipid profiles induced in the RXLI model were analysed using lipidomics as described in the Methods. We initially applied an untargeted approach to the whole lipid extracts from 3D epidermis. Only entities whose abundance appeared to be affected by the STS

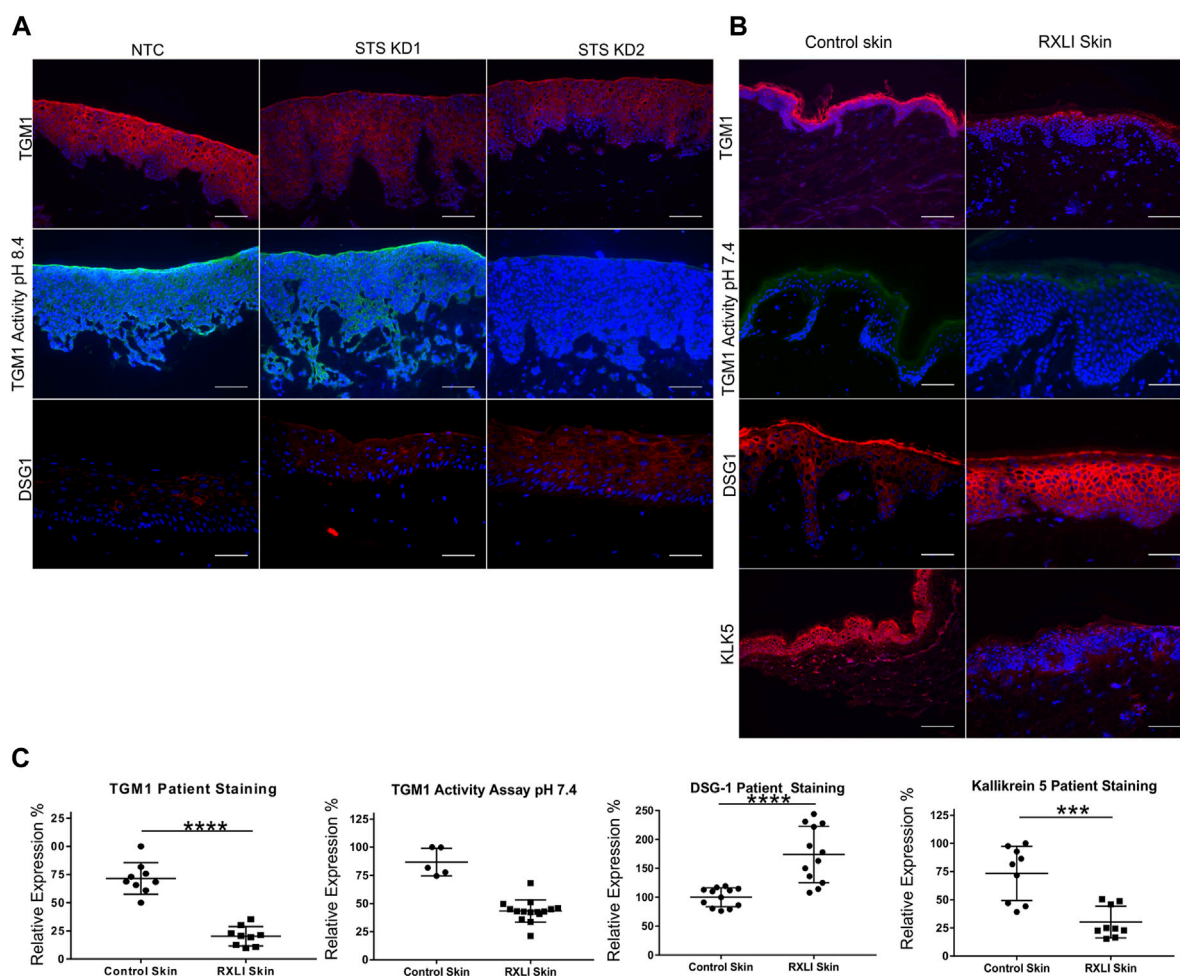


FIGURE 1

Loss of steroid sulfatase alters differentiation of the epidermis. (A) Immunohistochemistry of TGM1 expression in red (upper panel), TGM1 activity at pH 8.4 in green (middle panel) and DSG1 in red (lower panel) in 3D organotypics. (B) Immunohistochemistry of TGM1 expression (red) and activity at pH 7.4 (green), DSG1 (red) and KLK5 (green) expression in control skin and RXLI skin samples. DAPI (4',6-diamidino-2-phenylindole) nuclear staining is blue. (C) Quantification of immunostaining shown in (B). Three 40 X images were taken per sample ($n = 3$ for control and RXLI skin) for quantification of TGM1 and KLK5 expression. Five 40 X images were taken per sample ($n = 1$ for control skin and $n = 3$ for RXLI skin) for quantification of the TGM activity assay. Scale bar: 100 μm *** $p < 0.001$ and **** $p < 0.0001$ by unpaired 2-tailed t -test.

knockdown at a statistically significant extent were further processed for their identification. As shown in Figure 4A, CSO_4 expression was significantly increased in STS KD 2 epidermis, validating the model as CSO_4 retention is seen in RXLI. Principal component analysis (see Figure 4B) showed that there was a high degree of overlap between NTC and STS KD1, while there was an appreciable difference between NTC and STS KD2. The volcano plot in Figure 4C represents the changes of lipid levels in STS KD2 compared to NTC. Table 3 shows detailed changes that satisfied the cut-offs of fold change >1.4 and significance ≤ 0.05 in regulation of lipid species in STS KD2 versus NTC, as depicted in the volcano plot in Figure 4C. Supplementary Figure S3 shows hierarchical clustering of lipids modulated in STS KD1 and KD2 compared to NTC again confirming major changes in STS KD2 (lipid species are detailed in Supplementary Table S4). Several ceramide species belonging to the non-hydroxy fatty acyl dihydrosphingosine (NDS) subclass class consisting of non-hydroxy fatty acids (N) and dihydrosphingosine base (DS), which is also known

as sphinganine, were upregulated. Ceramide nomenclature is as described in these references (Masukawa et al., 2008; Liebisch et al., 2020). The increase of these ceramides may reflect a promoted *de novo* synthesis of ceramides or defective desaturation to the sphingosine base by sphingolipid desaturases, such as DEGS1. One member of the non-hydroxy fatty acyl sphingosine (NS) ceramides was upregulated. Ceramides containing deoxysphinganine as the sphingoid base were also upregulated. The increase of these anomalous ceramides may be due to condensation of alanine (instead of serine) with palmitoyl-CoA (Muthusamy et al., 2020). Several members of the tri hexosyl ceramides (Hex3Cer) were downregulated in KD2. Decreased levels of these sphingolipid metabolites in KD2 indicates deregulated sphingolipid synthesis/metabolism and trafficking (Iwabuchi et al., 2015). Moreover, the significantly decreased levels of N-acylphosphatidylethanolamine (NAPE) suggests deranged metabolism of endocannabinoids which may be related to the decrease of phosphatidylethanolamine (PE) species (Coulon et al., 2012). The significance of a moderate, but

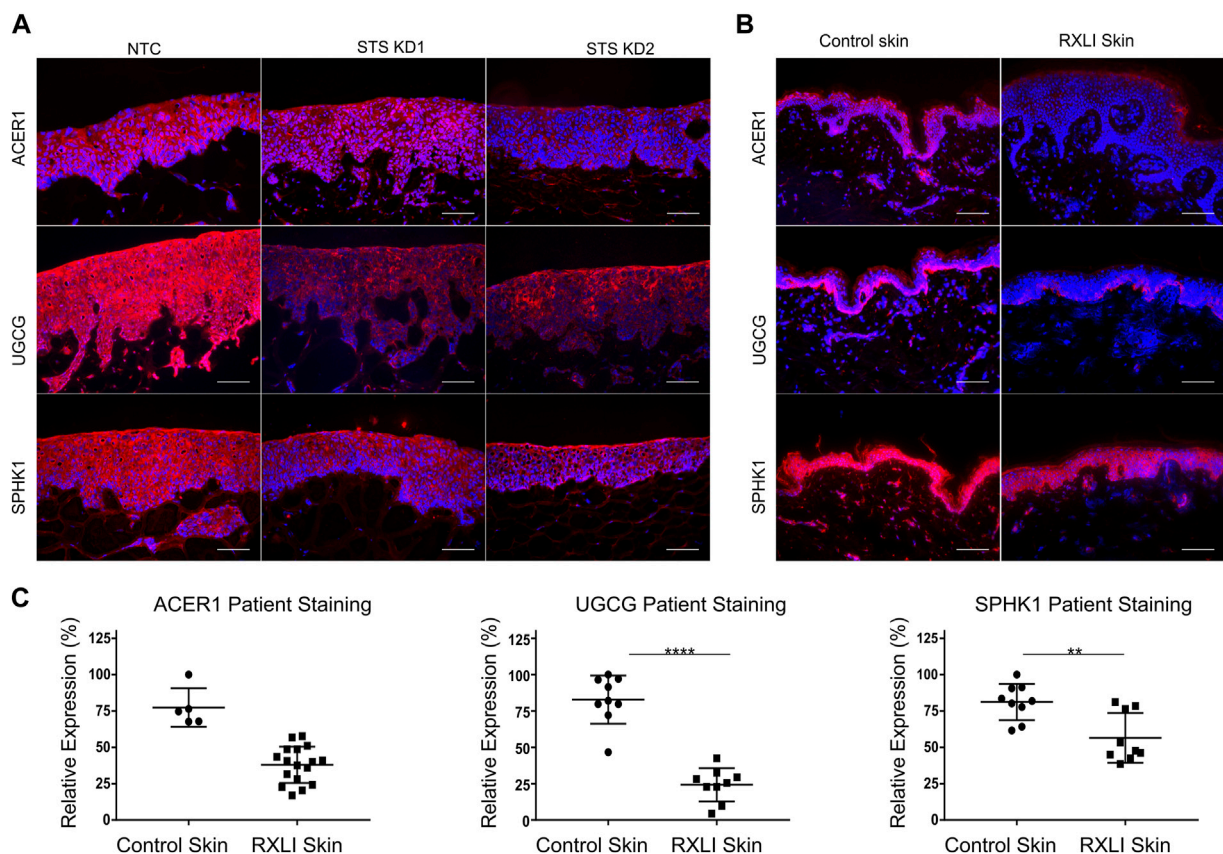


FIGURE 2

Loss of steroid sulfatase alters lipid metabolism in the epidermis. **(A)** Immunohistochemistry of ACER1, UGCG and SPHK1 expression in 3D organotypics. Scale bar: 100 μ m **(B)** Immunohistochemistry of ACER1, UGCG and SPHK1 expression in control skin and RXLI skin samples. All antigens of interest are in red. DAPI nuclear staining is blue. **(C)** Quantification of immunostaining shown in **(B)**. For UGCG and SPHK1 quantification three 40 X images were taken per sample ($n = 3$ each for control and RXLI skin). For ACER1 five 40 X images were taken per sample ($n = 1$ for control skin and $n = 3$ for RXLI skin). Scale bar: 100 μ m ** $p < 0.01$ and **** $p < 0.0001$ by unpaired 2-tailed t -test.

statistically significant, decrease of etherPEs requires further investigation (Fontaine et al., 2020).

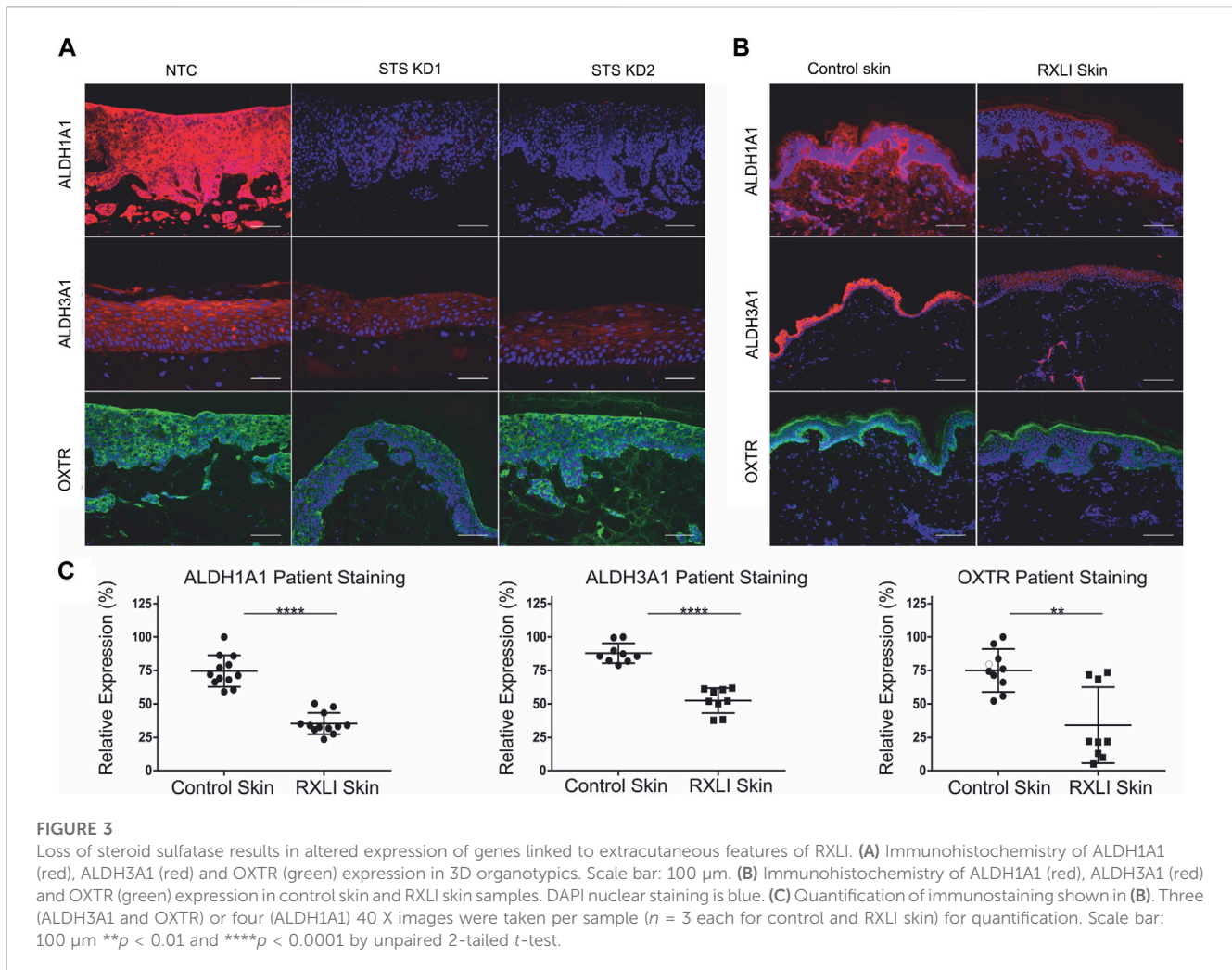
Discussion

Apart from deletion of *STS* and retention of CSO_4 , little is known about the underlying pathomechanisms in RXLI, or how extracutaneous phenotypes develop. These data further the understanding of RXLI pathomechanisms in skin, by showing loss of *STS* results in decreased expression of *TGM1*, *KLK5*, *ACER1*, *UGCG*, *SPHK1* and decreased *TGM* activity. Taken together, these data suggest *STS* is important for regulating epidermal homeostasis, lipid metabolism, proliferation, differentiation, and desquamation. The data presented also provide insights into pathomechanisms involved in corneal opacities, behavioural changes and prolonged labour in female carriers of RXLI. Although, we have not explored further, the presence of a gene cluster involved in cardiac septum morphogenesis may be relevant to the development of arrhythmias in some RXLI patients.

Mice with *Acer1* knockout have increased levels of ceramides and sphingomyelin, and decreased levels of sphingosine and sphingosine-1-phosphate (S1P). Furthermore, the mice have dry,

hyperplastic skin and a thickened stratum corneum (Liakath-Ali et al., 2016). The phenotype of these mice is similar to that of RXLI, particularly the dry skin and thickened stratum corneum, which suggests loss of *ACER1* contributes to RXLI skin pathology. The activity of *SPHK1* is crucial for generating S1P, which has anti-proliferative effects on keratinocytes (Di Nardo et al., 2000). Less *SPHK1* will generate less S1P, indicating the loss of *SPHK1* observed will result in a proliferative phenotype and altered differentiation.

A knockout mouse model of *Ugcg* presented with dry skin, thickening of the epidermis and hyperkeratosis, all phenotypes of RXLI. The knockout mice had extended expression of *K14* up through the suprabasal layers, and overexpression of *K6*, which would both indicate a proliferative phenotype (Amen et al., 2013) (Jennemann et al., 2007). Importantly, *Ugcg* knockout mice have reduced levels of free-extractable glucosylceramides and increased free-extractable ceramides. However, protein-bound ceramides are severely reduced, indicating *UGCG* is important for producing protein-bound ceramide precursors (protein-bound glucosylceramides). It is probable that the reduction of *UGCG* in RXLI would alter ceramide metabolism by lowering the glucosylceramide content of the epidermis, reflected by the decreased Hex3Cer shown in Table 3. As shown in mouse



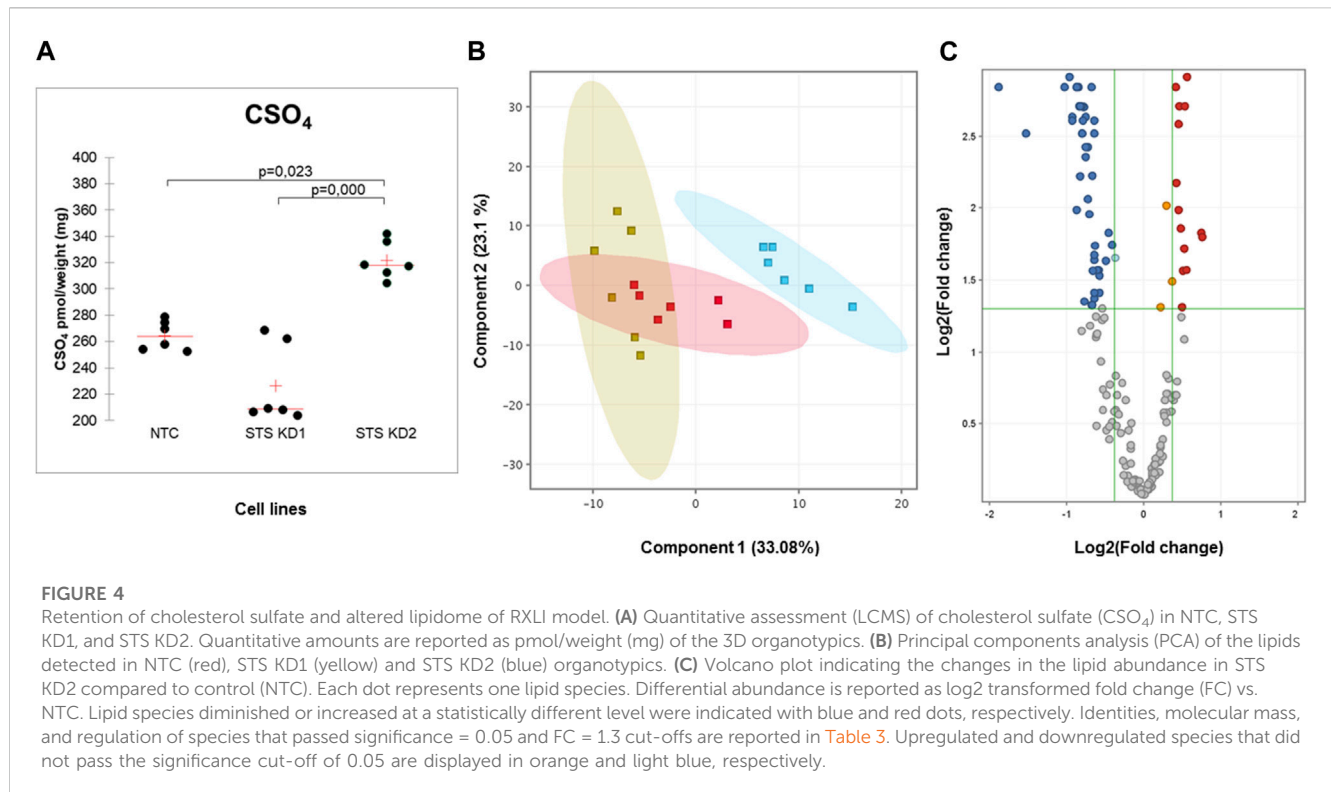
models, this would prevent the formation of protein bound ceramides, and impact on the cornified lipid envelope.

Both ALDH1A1 and ALDH3A1 are important in reducing UVR damage in the cornea and lens as their loss results in higher levels of ROS and thus damage to the eye. It is believed this is how the corneal opacities develop in *Aldh1a1/Aldh3a1* knockout mice (Lassen et al., 2007). It was also noted previously that knockdown of OXTR in keratinocytes and fibroblasts caused increased levels of ROS and decreased levels of glutathione, an important antioxidant (Deing et al., 2013). Therefore, loss of OXTR may also contribute to corneal opacities by further reducing the cornea's protection against stressors such as ultraviolet radiation. With our confirmation of reduced ALDH1A1, ALDH3A1 and OXTR expression in RXLI, we propose this is a contributing factor to the corneal opacities. Interestingly, the majority of corneal opacities in RXLI patients do not develop until the second or third decade of life. Damage caused by UVR may accumulate over time and act in combination with loss of these proteins in the development of corneal opacities, explaining why these develop later in life. As only half of patients develop corneal opacities, there may be other genetic or environmental factors involved. The aldehyde dehydrogenase family members

are important components of the retinoic acid signalling pathway which is important in regulating epithelial proliferation (Kumar et al., 2017). A reduction in ALDH1A1 and ALDH3A1 may also affect keratinocyte proliferation.

Behaviours on the autistic spectrum and ADHD are more common in RXLI patients (25% and 40%, respectively) than the general population (Kent et al., 2008; Deing et al., 2013). It has been shown that loss of STS due to point mutations alone can result in RXLI patients developing ADHD. Interestingly, dysregulation of ceramides, alkaline ceramidases and S1P have been implicated in neurodegenerative disorders, indicating the potentially altered sphingolipids in RXLI may contribute to the behavioural disorders associated with RXLI (Cutler et al., 2004; Ben-David and Futerman, 2010; Wang et al., 2015). There are now numerous studies which conclude that polymorphisms in the *OXTR* gene confer a risk of behavioural disorders (Jacob et al., 2007; Lerer et al., 2008; Liu et al., 2010). It is theorised this is a result of oxytocin being unable to properly elicit its neurological effects due to loss of its receptor.

In RXLI, reduced placental STS results in prolonged labour. Oxytocin is used to induce uterine contractility (Fuchs et al., 1982). A reduction of placental OXTR expression may contribute to prolonged labour. Transport of OXT has been shown to occur from mother to



foetus and *vice versa*, which helps explain how loss of OXTR due to RXLI could potentially affect the mother and parturition regulation (Malek, Blann, and Mattison, 1996). This reduction of OXTR could be a result of decreased oestrogen, or a concurrent mechanism that also contributes to prolonged parturition.

In summary, in this paper, we show that loss of STS in human epidermis causes major changes to ceramide and sphingolipid synthesis. This expands our understanding of RXLI pathogenesis and has implications for the skin barrier. The changes in sphingolipids may also be associated with the neuropsychiatric symptoms experienced by these patients. The connection between ALDH1A1 and ALDH3A1 loss and corneal opacities, and OXTR loss and prolonged labour and behavioural disorders provides a new explanation for the extracutaneous features of RXLI. In addition, the RNA-Seq data showed altered RNA expression of several genes linked to behavioural disorders and brain and cardiac development which could be explored further. Further work could be performed in a mouse model or using patient-derived induced pluripotent stem cells which could be differentiated into cells of interest including cardiomyocytes or neurons. A better understanding of the biological mechanisms underlying RXLI may lead to new treatments in the future.

Materials and methods

Study approval

This study was conducted according to the Declaration of Helsinki Principles and was approved by the East London and

City Health Authority Research Ethics Committee. Written informed consent was obtained from patients before samples were taken.

Control skin samples and RXLI skin samples

Dermal fibroblasts were isolated from neonatal foreskins. Redundant normal skin was used as a control for RXLI skin samples. Samples of RXLI skin were obtained from 3 individuals diagnosed with RXLI, confirmed by either steroid sulfatase activity assays or genetic testing.

Cell culture and Knockdown cell lines

The human keratinocyte telomerase reverse-transcriptase-immortalized (h/TERT-immortalized) N/TERT-1 cell line derived from clinically normal foreskin tissue and supplied by James Rheinwald (Department of Dermatology, Harvard University Medical School, Boston, Massachusetts, United States) (Dickson et al., 2000) was grown in RM + growth media (DMEM/F-12, 10% FBS, 1× penicillin streptomycin [P/S], 0.4 µg/mL hydrocortisone, 0.5 µg/mL insulin, 10 ng/mL epidermal growth factor, 0.1 nM cholera toxin, 5 µg/mL transferrin, 20 p.m. liothyronine) and incubated at 37°C, 5% CO₂. Human primary fibroblasts isolated from fresh redundant skin were grown in fibroblast growth media (DMEM, 10% FBS, 1× P/S) and incubated at 37°C, 5% CO₂. Primary keratinocytes were isolated from neonatal foreskin and grown in Epilife media. SMARTvector

TABLE 3 Lipid species upregulated and downregulated in STS KD2 cells compared to control.

Compound	Mass	FC (STS KD2 Vs. NTC)	Log FC (STS KD2 Vs. NTC)	Regulation (STS KD2 Vs. NTC)
Cholesterol sulfate	466,3115	1,49	0,57	up
Cer(d18:0/22:0)	623,6191	1,45	0,53	up
Cer(d18:0/24:0)	651,6520	1,40	0,49	up
Cer(d18:0/26:0)	679,6835	1,38	0,46	up
Cer(d18:0/28:0)	707,7141	1,34	0,42	up
Cer(d18:1/22:0)	621,6017	1,42	0,51	up
Cer(m18:0/20:0)	579,5908	1,42	0,50	up
Cer(m18:0/22:0)	607,6240	1,48	0,56	up
Cer(m18:0/24:0)	635,6570	1,46	0,54	up
Cer(m18:0/24:1)	633,6417	1,37	0,46	up
Cer(m18:0/26:0)	663,6881	1,34	0,43	up
Cer(m18:0/26:1)	661,6730	1,37	0,46	up
EtherPC 40:2	827,6639	1,69	0,75	up
SM 40:2;O2	784,6430	1,70	0,76	up
NAPE(48:2)	925,7069	-1,56	-0,64	down
Hex3Cer(d18:0/14:1)	995,6363	-1,32	-0,41	down
Hex3Cer(d18:0/16:1)	1023,670	-1,71	-0,78	down
Hex3Cer(d18:0/18:1)	1051,699	-1,48	-0,57	down
Hex3Cer(d18:0/20:1)	1079,731	-1,48	-0,57	down
Hex3Cer(d18:0/24:1)	1135,794	-1,60	-0,68	down
Hex3Cer(d18:1/14:0)	995,6363	-1,36	-0,45	down
Hex3Cer(d18:1/16:0)	1023,670	-1,71	-0,77	down
Hex3Cer(d18:1/18:0)	1051,699	-1,56	-0,64	down
Hex3Cer(d18:1/18:1)	1023,670	-1,71	-0,78	down
Hex3Cer(d18:1/20:0)	1079,730	-1,50	-0,58	down
Hex3Cer(d18:1/20:1)	1051,699	-1,54	-0,63	down
Hex3Cer(d18:1/24:0)	1135,794	-1,59	-0,66	down
Hex3Cer(d18:1/24:1)	1133,778	-1,82	-0,87	down
Hex3Cer(d18:1/26:1)	1161,809	-1,70	-0,76	down
PE 31:2	673,4664	-1,58	-0,66	down
PE 32:1	689,5011	-1,60	-0,67	down
PE 32:0	691,5161	-1,55	-0,63	down
PE 34:4	711,4799	-1,56	-0,64	down
PE 34:3	713,5015	-1,62	-0,70	down
PE 34:2	715,5223	-1,89	-0,92	down
PE 34:1	717,5291	-1,94	-0,96	down
PE 35:5	727,5234	-1,51	-0,59	down
PE 36:4	739,5121	-1,73	-0,79	down

(Continued on following page)

TABLE 3 (Continued) Lipid species upregulated and downregulated in STS KD2 cells compared to control.

Compound	Mass	FC (STS KD2 Vs. NTC)	Log FC (STS KD2 Vs. NTC)	Regulation (STS KD2 Vs. NTC)
PE 36:3	741,5337	-1,68	-0,75	down
PE 36:2	743,5466	-2,03	-1,02	down
PE 36:1	745,5616	-1,89	-0,92	down
PE 38:4	767,5443	-1,71	-0,78	down
PE 38:3	769,5597	-1,77	-0,82	down
PE 38:2	771,5786	-1,78	-0,83	down
PE 40:8	787,5107	-1,55	-0,63	down
PE 40:7	789,5289	-1,68	-0,75	down
PE 40:6	791,5450	-1,79	-0,84	down
EtherPE 32:2	673,5048	-1,55	-0,63	down
EtherPE 34:3	699,5168	-1,65	-0,72	down
EtherPE 34:2	701,5359	-1,57	-0,65	down
EtherPE 36:6	721,5056	-1,82	-0,87	down
EtherPE 36:5	723,5194	-1,74	-0,80	down
EtherPE 36:4	725,5350	-1,64	-0,72	down
EtherPE 36:2	729,5682	-1,77	-0,82	down
EtherPE 38:6	749,5345	-1,77	-0,82	down
EtherPE 38:5	751,5484	-1,73	-0,79	down
EtherPE 40:7	775,5501	-1,68	-0,75	down
EtherPE 40:6	777,5673	-1,82	-0,86	down
SM 32:1;O2	674,5364	-1,40	-0,49	down

2.0 lentiviral shRNA particles (GE Healthcare, UK) targeting exons five and ten were used to transduce N/TERT keratinocytes with an shRNA construct in order to generate a stable knockdown of STS (see [Supplementary Table S1](#)). A non-targeting shRNA construct was transduced into keratinocytes and used as a control. The construct included a GFP reporter to allow confirmation of successful transduction.

3D model of RXLI

Collagen and Matrigel gels were prepared by mixing 3.5 volumes of collagen I with 3.5 volumes of Matrigel, one volume of MEM, one volume of FBS and 1 volume of primary fibroblasts. 1 ml of gel mix was added per well required of a 24 well plate and incubated at 37°C for 1 h. Subsequently, 1 ml of media were added to the top of the gel and incubated overnight at 37°C. The media were aspirated from the gel, and N/TERT keratinocytes infected with shRNA lentiviral particles were seeded on top of the gel and incubated at 37°C overnight. The gels were then raised to the air/liquid interface on a steel grid placed in a 6 well plate. The gels were incubated for a further 14 days.

Preparation of tissues

Tissues were fixed in 4% PFA and embedded in paraffin using an automated tissue processor. Sections (5 µm-thick) of 4% PFA-fixed and paraffin embedded samples were cut using a Reichert-Jung 2035 microtome and placed on SuperFrost Plus slides. Sections were then deparaffinized in xylene and then rehydrated through a graduated ethanol series and water before immunostaining. Cryosections (10 µm-thick) of frozen samples mounted in OCT (Tissue-Tek, NL) were cut in a cryostat, placed on SuperFrost Plus slides and stored at -80°C. When used, sections were left to air dry for 10 min then washed once in PBS before immunostaining.

Immunostaining

Sections were washed in PBS for 5 min, then blocked by incubating in IFF (1% BSA w/v, 2% FBS v/v in PBS) containing 5%–10% goat serum for 1 hour. Sections were then probed with primary antibody diluted in PBS containing 1% BSA and incubated on the section at RT for 2 hours or overnight at 4°C. Sections were washed three times with PBS before

addition of the secondary antibody, Alexa Fluor 568-red or 488-green, goat anti-rabbit or goat anti-mouse (Invitrogen, CA, United States) at a 1:500 dilution for 1 hour at room temperature. Sections were washed three times in PBS before DAPI at a 1:1000 dilution was used as a nuclear stain. Following a further three washes in PBS the sections were mounted using Immu-mount (Thermo Fisher Scientific MA, United States). Negative controls consisted of mouse or rabbit IgG diluted to the same concentration as the primary antibody. Images were obtained using a Leica MM epi-fluorescence microscope. Antibodies used are detailed in [Supplementary Table S2](#).

Transglutaminase assay

Cryosections were washed with PBS for 5 min. Four sections were used per sample. Sections were blocked by incubation in 0.1 M Tris with 3% BSA at either pH 7.4 or pH 8.4. Sections were then incubated with 0.1 M Tris with 3% BSA containing either 20 μ l 10 mM biotinylated monodansylcadaverine +20 μ l 0.5 M CaCl₂ per ml (positive sample) or 20 μ l 10 mM biotinylated monodansylcadaverine +20 μ l 0.5 M EDTA per ml (negative sample) at either pH 7.4 or pH 8.4 for 1 hour. The reaction was stopped by incubation of sections for 10 min with PBS +20 μ l 0.5 M EDTA per ml. The sections were then washed three times with PBS. Streptavidin-Alexa488 diluted 1:2000 and DAPI diluted 1:1000 in PBS was applied to the sections for 30 min. The sections were then washed a further three times and mounted using Immu-mount. Images were obtained using a Leica MM epi-fluorescence microscope.

Quantification

The staining of RXLI patient and normal control skin was quantified using Cell Profiler (3.0.0) which measured the intensity of staining across each image taken. This allowed us to calculate an average intensity per cell for control skin samples and RXLI patient samples, which were then averaged across multiple images from the same section to produce an overall value.

RNA work

Total RNA was extracted from cells in a six well plate and purified using the RNeasy kit (Qiagen, NL) according to the manufacturer's instructions. Concentration of RNA samples was determined by measuring the absorbance at 260 nm with a spectrophotometer after RNA extraction (Nanodrop, ND-1000 Spectrophotometer) and stored at -80°C . cDNA was synthesised from total RNA using SuperScript VILO cDNA synthesis kit (Invitrogen, CA, United States) according to the manufacturer's instructions.

qPCR

The qPCR was performed with 5 ng of cDNA using the KAPA SYBR FAST qPCR kit (Biosystems, ES). cDNA was mixed with 1x

KAPA SYBR FAST qPCR Master Mix, forward primer (200 nM), reverse primer (200 nM), and carboxy-X-rhodamine (ROX) reference dye low. The mix was adjusted to a reaction volume of 10 μ l with water. The qPCR reaction was carried out using the 7,500 Real Time PCR system (Life Technologies, CA, United States) with the following cycle sequence: initiation at 95°C for 5 min, then 40 cycles of melting at 95°C for 10 s, annealing at 60°C for 30 s, and extension at 72°C for 40 s. Each sample was analysed in triplicate and data analysis was performed using the 7,500 System Detection Software v1.4 (Life Technologies, CA, United States) and Microsoft Excel 2011. HPRT was used as an internal control. Primers used are detailed in [Supplementary Table S3](#).

RNA Sequencing

HISAT2 was used to align sequencing reads to a reference genome. This tool uses the Burrows-Wheeler transform and the FM index to align reads with Bowtie2 as the algorithmic core. Once the reads are aligned, HTSeq is used to produce counts for each gene of how many aligned reads overlap its exons. This preprocesses the RNA-Seq data for differential expression analysis. The counts are fed into DESeq2, a tool used for differential expression analysis based on a model using negative binomial distribution.

Statistics

Statistical analysis was determined by a Student's unpaired two-tailed *t*-test using GraphPad Prism 7.03 (GraphPad Software). A *p*-value of 0.05 or less was considered statistically significant.

Sample processing for the analysis of lipids

Organotypics (NTC, $n = 3$, STS KD1 $n = 3$, and STS KD2 $n = 3$) were treated as a whole. Organotypics were weighed and lipids extracted with a chloroform/methanol mixture 2:1 after addition of the internal standard mixture containing SPLASH Lipidomix[®], LM6002, and d31CerNS (Avanti Polar Lipids, United States), and in-house mixed deuterated standards supplied by C/D/N isotopes and Toronto Research Chemicals, both from Canada. Aliquots of dissolved lipid extracts were analysed in duplicate by GCMS for the quantification of cholesterol, desmosterol, and free fatty acids. The dissolved lipid extracts were further analysed in duplicate by untargeted LCMS in positive and negative ion mode. The results of the untargeted approach were normalised by the internal standard d31CerNS and the weight of each sample. Quantitative results from both GCMS and LCMS were normalised by the mg of tissue weight and reported as pmol/weight (mg of tissue).

Gas chromatography-mass spectrometry

Gas chromatography coupled to electron ionisation mass spectrometry (GCMS) dual scan-selected ion monitoring was employed to determine target compounds in the lipid extracts.

Samples were analysed with a GC 7890 A coupled to the MS 5975 VL analyzer (Agilent Technologies, CA, United States). Analysis of free cholesterol was performed simultaneously to free fatty acids (FFAs) analysis by a GCMS method as previously reported (Singh et al., 2018). 20 μ L of the lipid extracts dissolved in 200 μ L of $\text{CHCl}_3/\text{MeOH}$ 2:1 mixture were dried under nitrogen and derivatized with 50 μ L BSTFA added with 1% trimethylchlorosilane (TCMS) in pyridine to generate the trimethylsilyl (TMS) derivatives. The reaction was carried out at 60°C for 60 min. GC separation was performed with the 30 m–0.250 (i.d.) GC DB-5MS UI fused silica column (Agilent Technologies, CA, United States), chemically bonded with a 5% diphenyl 95% dimethylpolysiloxane cross-linked stationary phase (0.25 mm film thickness). Helium was used as the carrier gas. Samples were acquired in scan mode by means of electron impact (EI) MS. Cholesterol and FFAs were determined against d7Cholesterol and d31C16:0, respectively, with the MassHunter quantitative software (Agilent Technologies, CA, United States). Analyses were run in duplicate.

Liquid chromatography-mass spectrometry

The chromatographic apparatus consisted of the 1260 Infinity II series LC system (Agilent Technologies, CA, United States). High resolution reversed phase liquid chromatography (RPLC) was performed with a Zorbax SB-C8 HT (2.1 \times 100 mm, 1.8 μ m p. s.) with a maximal operational backpressure at 600 Bar (Agilent Technologies, CA, United States). Lipid mixtures were eluted a gradient of (A) 5 mM ammonium formate in water, (B) methanol, (C) acetonitrile, (D) isopropanol. The elution program was as follows: A/B/C/D 60/28/8/40 at time 0 and held for 1 min, brought to A/B/C/D 1/70/20/9 in 10 min and held up to 20 min. The flow rate was maintained at 400 μ L/min during the entire LC run. The column was thermostated at 60°C. The injection volume was 0.20 μ L. The separation of polar lipids, e.g., phosphatidylcholines (PCs), phosphatidylethanolamins (PEs), and sphingomyelins (SMs), was performed on a HILIC stationary phase. The HaloHILIC column (2.1 \times 50 mm, 2.7 μ m p. s.) was purchased from Advanced Materials Technologies (PN 9281-1204, Wilmington, DE, US). The separation of lipids in HILIC mode was performed with a gradient of (A) 5 mM ammonium formate in water, (B) methanol, and (C) acetonitrile. The elution program was as follows: A/B/C 1/2/97 at time 0 and held for 1 min, brought to A/B/C 18/2/80 in 20 min and held up to 10 min. The flow rate was maintained at 400 μ L/min during the entire LC run. The column was thermostated at 40°C. The injection volume was 1 μ L. The mobile phases were filtered through 0.45 μ m glass filters and continuously degassed under vacuum. The injector needle was washed with the mobile phase in the wash port during the LC runs.

Accurate mass measurements in full MS and auto MS/MS were conducted with a G6545B series LC-QTOF (Agilent Technologies, United States) equipped with a JetStream Technology electrospray interface (ESI) interface operating in both positive and negative ion mode. Analytes eluted from the LC system were introduced into the

Q-TOF apparatus at the operating chromatographic flow rate (see chromatographic conditions). Nitrogen was used as the nebulizing and desolvation gas. The temperature and the flow of the drying gas temperature were 200°C, and 12 L/min, respectively. The temperature and the flow of the sheath gas were 350°C and 12 L/min, respectively. The nebulizer pressure was 40 psi. The capillary and the fragmentor voltage were 4,000 and 180 V, respectively. Full scan mass spectra were acquired in the positive and negative ion modes in the range from m/z 100 to m/z 1600. To enhance accurate mass measurement for the ion species a reference solution of two compounds with m/z 121.050873 and 922.009798, respectively, was vaporized in continuum in the spray chamber by means of a separate nebulizer. Analyses were performed in duplicate in each mode.

Extraction of MS features

Molecular features, defined by an m/z, RT and signal intensity value, were extracted from the raw LCMS data files using the untargeted or the targeted batch recursive feature extraction in the MassHunter Profinder software (Agilent Technologies, United States). The features extracted were exported into a compound exchange format (CEF) reporting RT, the accurate mass and the absolute abundance for each entity to be processed in the subsequent chemometric analysis as previously reported (Ludovici et al., 2018; Singh et al., 2018).

Data analysis (lipidomics)

Agilent Mass Profiler Professional (MPP version 15.1) was used to process the LCMS untargeted and targeted data. Retention times (RT) were aligned by setting a RT window of 0.6 min, whereas m/z binning was performed by setting windows at 10 ppm. Absolute abundance of each entity was normalised by the absolute abundance of the d31CerNS internal standard. Data were filtered by frequency of detection, which reflects the number of samples that presented particular features. A frequency filter was applied to data extracted from MPP and only entities present in 100% of samples belonging to at least one of the investigated groups were retained for the statistical analysis. Fold changes of filtered entities were compared between groups volcano plots in the MPP tools. Fold changes with *p* values <0.05 after Bonferroni's correction were considered as significant. Identification of entities within the MPP workflow was performed based on the METLIN Metabolomics Database (<http://metlin.scripps.edu/>) and the Lipid Annotator software (Agilent Technologies, CA, United States). Quantitative assessment of cholesterol sulfate (CSO_4) was performed with the deuterium labelled internal standard d7 CSO_4 .

Data availability statement

The data presented in this study are deposited in the NIH GEO repository under GSE 232622.

Ethics statement

The studies involving human participants were reviewed and approved by East London and City Health Authority. The patients/participants provided their written informed consent to participate in this study.

Author contributions

This project was conceived by EO who obtained funding. EO, EC, and AE supervised the work. MC helped with day to day supervision. All of the experimental work was performed by FM, PD, MMe, EC, and MMA. Patients were recruited and biopsied by SZ and EO. The manuscript was written by FM, EC and EO with comments by all the authors. All authors contributed to the article and approved the submitted version.

Funding

The study was funded by a BBSRC CASE studentship with Glaxo Smith Kline (BB/L502303/1) which funded FMG and a project grant from Action Medical Research (Grant No: GN2547) which funded MH.

Acknowledgments

We would like to acknowledge the Blizzard Advanced Light Microscopy Facility staff. We would like to acknowledge Glaxo Smith Kline scientists that performed the RNA sequencing and

References

- Amen, N., Mathow, D., Rabionet, M., Sandhoff, R., Langbein, L., Gretz, N., et al. (2013). Differentiation of epidermal keratinocytes is dependent on glucosylceramide: ceramide processing. *Hum. Mol. Genet.* 22 (20), 4164–4179. doi:10.1093/hmg/ddt264
- Arrowsmith, S., and Wray, S. (2014). Oxytocin: Its mechanism of action and receptor signalling in the myometrium. *J. Neuroendocrinol.* 26. doi:10.1111/jne.12154
- Baek, H. S., Kwon, T. U., Shin, S., Kwon, Y. J., and Chun, Y. J. (2021). Steroid sulfatase deficiency causes cellular senescence and abnormal differentiation by inducing yippee-like 3 expression in human keratinocytes. *Sci. Rep.* 11 (1). doi:10.1038/s41598-021-00051-w
- Barrett, T., Stephen, E., Wilhite, P. L., Irene, F., Kim, M. T., Kimberly, A., et al. (2013). NCBI GEO: Archive for functional genomics data sets—update. *Nucleic Acids Res.* 41, D991–D995. doi:10.1093/nar/gks1193
- Ben-David, O., and Futerman, A. H. (2010). The role of the ceramide acyl chain length in neurodegeneration: Involvement of ceramide synthases. *Neuromolecular Med.* 12 (4), 341–350. doi:10.1007/s12017-010-8114-x
- Brcic, L., Georgina, H., WrenUnderwood, J. F. G., Kirov, G., and Davies, W. (2022). Comorbid medical issues in X-linked ichthyosis. *JID Innovations Skin Sci. Mol. Popul. Health* 2 (3), 100109. doi:10.1016/j.xjidi.2022.100109
- Brcic, L., Kendall, K. M., Caseras, X., Kirov, G., and Davies, W. (2020). Medical and neurobehavioural phenotypes in carriers of X-linked ichthyosis-associated genetic deletions in the UK Biobank. *J. Med. Genet.* 57 (10), 692–698. doi:10.1136/jmedgenet-2019-106676
- Caubet, C., Jonca, N., Brattsand, M., Guerrin, M., Bernard, D., Schmidt, R., et al. (2004). Degradation of corneodesmosome proteins by two serine proteases of the kallikrein family, SCFE/KLK5/hK5 and SCCE/KLK7/hK7. *J. Investigative Dermatology* 122 (5), 1235–1244. doi:10.1111/j.0022-202X.2004.22512.x
- Cavenagh, A., Chatterjee, S., and Davies, W. (2019). Behavioural and psychiatric phenotypes in female carriers of genetic mutations associated with X-linked ichthyosis. *PLoS One* 14 (2), e0212330. doi:10.1371/journal.pone.0212330
- Coulon, D., Faure, L., Salmon, M., Wattelet, V., and Bessoule, J. J. (2012). Occurrence, biosynthesis and functions of N-acylphosphatidylethanolamines (NAPE): Not just precursors of N-acyl ethanolamines (NAE). *Biochimie* 94 (1), 75–85. doi:10.1016/j.biochi.2011.04.023
- Craig, W. Y., Roberson, M., Palomaki, G. E., Shackleton, C. H. L., Marcos, J., and Haddow, J. E. (2010). Prevalence of steroid sulfatase deficiency in California according to race and ethnicity. *Prenat. Diagn.* 30 (9), 893–898. doi:10.1002/pd.2588
- Crane, J. S., and Paller, A. S. (2022). “X-linked ichthyosis,” in *StatPearls* (St. Petersburg, FL, USA: Treasure Island (FL): StatPearls Publishing).
- Cutler, R. G., Kelly, J., Storie, K., Ward, A., Pedersen, A. T., Troncoso, J. C., et al. (2004). Involvement of oxidative stress-induced abnormalities in ceramide and cholesterol metabolism in brain aging and alzheimer’s disease. *Proc. Natl. Acad. Sci. U. S. A.* 101 (7), 2070–2075. doi:10.1073/pnas.0305799101
- Deing, V., Roggenkamp, D., Kühnl, J., Gruschka, A., Stäb, F., Wenck, H., et al. (2013). Oxytocin modulates proliferation and stress responses of human skin cells: Implications for atopic dermatitis. *Exp. Dermatol.* 22 (6), 399–405. doi:10.1111/exd.12155
- Di Nardo, A., Benassi, L., Magnoni, C., Cossarizza, A., Seidenari, S., and Giannetti, A. (2000). Ceramide 2 (N-acetyl sphingosine) is associated with reduction in bcl-2 protein levels by western blotting and with apoptosis in cultured human keratinocytes. *Br. J. Dermatology* 143 (3), 491–497. doi:10.1111/j.1365-2133.2000.03700.x
- Dickson, M. A., Hahn, W. C., Ino, Y., Ronfard, V., Wu, J. Y., Weinberg, R. A., et al. (2000). Human keratinocytes that express hTERT and also bypass a p16(INK4a)-enforced mechanism that limits life span become immortal yet retain normal growth and differentiation characteristics. *Mol. Cell. Biol.* 20 (4), 1436–1447. doi:10.1128/MCB.20.4.1436-1447.2000
- Diociaiuti, A., Angioni, A., Pisaneschi, E., Alesi, V., Zambruno, G., Novelli, A., et al. (2019). X-linked ichthyosis: Clinical and molecular findings in 35 Italian patients. *Exp. Dermatol.* 28 (10), 1156–1163. doi:10.1111/exd.13667

supported the project. We are grateful to Dr Harpreet Kaur Saini who helped with early analysis of the RNA sequencing data.

Conflict of interest

EO has had grant funding from Palvella Therapeutics and Kamari Pharma. She has consulted for Palvella Therapeutics, Kamari Pharma and Azitra Inc. She has had PhD studentships co-funded with GSK and Unilever. She has been a speaker for Almirall. All money goes to the university. MD was employed by Senzo Health Limited.

The remaining authors declare that the research was conducted in the absence of any commercial or financial relationships that could be construed as a potential conflict of interest.

Publisher’s note

All claims expressed in this article are solely those of the authors and do not necessarily represent those of their affiliated organizations, or those of the publisher, the editors and the reviewers. Any product that may be evaluated in this article, or claim that may be made by its manufacturer, is not guaranteed or endorsed by the publisher.

Supplementary material

The Supplementary Material for this article can be found online at: <https://www.frontiersin.org/articles/10.3389/fmolb.2023.1176802/full#supplementary-material>

- Fontaine, D., Figiel, S., Félix, R., Kouba, S., Fromont, G., Mahéo, K., et al. (2020). Roles of endogenous ether lipids and associated PUFAs in the regulation of ion channels and their relevance for disease. *J. Lipid Res.* 61 (6), 840–858. doi:10.1194/jlr.RA120000634
- Fuchs, A. R., Fuchs, F., Husslein, P., Soloff, M. S., Fernström, M. J., and Pearson, J. F. (1982). Oxytocin receptors and human parturition. *Obstet. Anesth. Dig.* 215. doi:10.1097/00132582-198209000-00007
- Iwabuchi, K., Nakayama, H., Oizumi, A., Suga, Y., Ogawa, H., and Takamori, K. (2015). Role of ceramide from glycosphingolipids and its metabolites in immunological and inflammatory responses in humans. *Mediat. Inflamm.* 2015, 120748. doi:10.1155/2015/120748
- Jacob, S., Brune, C. W., Carter, C. S., BennettLeventhal, L., Lord, C., and Cook, E. H. (2007). Association of the oxytocin receptor gene (OXTR) in caucasian children and adolescents with autism. *Neurosci. Lett.* 417 (1), 6–9. doi:10.1016/j.neulet.2007.02.001
- Jennemann, R., Sandhoff, R., Langbein, L., Kaden, S., Rothermel, U., Gallala, H., et al. (2007). Integrity and barrier function of the epidermis critically depend on glucosylceramide synthesis. *J. Biol. Chem.* 282 (5), 3083–3094. doi:10.1074/jbc.M610304200
- Kent, L., Emerton, J., Bhadravathi, V., Weisblatt, E., Pasco, G., Willatt, L. R., et al. (2008). X-linked ichthyosis (steroid sulfatase deficiency) is associated with increased risk of attention deficit hyperactivity disorder. *Autism Soc. Commun. Deficits.* *J. Med. Genet.* 45 (8), 519–524. doi:10.1136/jmg.2008.057729
- Koppe, G., Marinkovic-Ilsen, A., Rijken, Y., De Groot, W. P., and Jobsis, A. C. (1978). X-linked ichthyosis. A sulphatase deficiency. *Archives Dis. Child.* 53. doi:10.1136/ad.53.10.803
- Kumar, S., Pascal, D., Ghyselinck, N. B., and Duyster, G. (2017). Endogenous retinoic acid signaling is required for maintenance and regeneration of cornea. *Exp. Eye Res.* 154, 190–195. doi:10.1016/j.exer.2016.11.009
- Lassen, N., Bronwyn Bateman, J., Jer, R., David, W., Nees, J. P., Gregg, D., et al. (2007). Multiple and additive functions of ALDH3A1 and ALDH1A1: Cataract phenotype and ocular oxidative damage in *aldh3a1(-/-)/aldh1a1(-/-)* knock-out mice. *J. Biol. Chem.* 282. doi:10.1074/jbc.M702076200
- Lerer, E., Levi, S., Salomon, S., Darvasi, A., Yirmiya, N., and Ebstein, R. P. (2008). Association between the oxytocin receptor (OXTR) gene and autism: Relationship to vineland adaptive behavior scales and cognition. *Mol. Psychiatry* 13 (10), 980–988. doi:10.1038/sj.mp.4002087
- Liakath-Ali, K., Valerie, E. V., Christopher, J. L., Anneliese, O., Speak, D. L., Hayley, J. P., et al. (2016). Alkaline ceramidase 1 is essential for mammalian skin homeostasis and regulating whole-body energy expenditure. *J. Pathology* 239 (3), 374–383. doi:10.1002/path.4737
- Liebisch, G., Eoin, F., JunkenEdward, A., Dennis, T., Durand, C. S., Ejsing, M. F., et al. (2020). Update on LIPID MAPS classification, nomenclature, and shorthand notation for MS-derived lipid structures. *J. Lipid Res.* 61 (12), 1539–1555. doi:10.1194/jlr.S120001025
- Liu, X., Kawamura, Y., Shimada, T., Otowa, T., Koishi, S., Sugiyama, T., et al. (2010). Association of the oxytocin receptor (OXTR) gene polymorphisms with autism spectrum disorder (ASD) in the Japanese population. *J. Hum. Genet.* 55 (3), 137–141. doi:10.1038/jhg.2009.140
- Ludovici, M., Kozul, N., Materazzi, S., Risoluti, R., Picardo, M., and Camera, E. (2018). Influence of the sebaceous gland density on the stratum corneum lipidome. *Sci. Rep.* 8 (1), 11500.
- Malek, A., Blann, E., and Mattison, D. R. (1996). Human placental transport of oxytocin. *J. Maternal-Fetal Neonatal Med. Official J. Eur. Assoc. Perinat. Med. Fed. Asia Ocean. Perinat. Soc. Int. Soc. Perinat. Obstetricians* 5 (5), 245–255. doi:10.1002/(SICI)1520-6661(199609/10)5:5<245:AID-MFM3>3.0.CO;2-H
- Masukawa, Y., Narita, H., Shimizu, E., Kondo, N., Sugai, Y., Oba, T., et al. (2008). Characterization of overall ceramide species in human stratum corneum. *J. Lipid Res.* 49 (7), 1466–1476. doi:10.1194/jlr.M800014-JLR200
- Muthusamy, T., Thekla Cordes, M., Handzlik, K., Esther, W., Lim, J. G., Antonio, F. M., et al. (2020). Serine restriction alters sphingolipid diversity to constrain tumour growth. *Nature* 586 (7831), 790–795. doi:10.1038/s41586-020-2609-x
- Nemes, Z., Demény, M., Marekov, L. N., Fésüs, L., and Steinert, P. M. (2000). Cholesterol 3-sulfate interferes with cornified envelope assembly by diverting transglutaminase 1 activity from the formation of cross-links and esters to the hydrolysis of glutamine. *J. Biol. Chem.* 275 (4), 2636–2646. doi:10.1074/jbc.275.4.2636
- Paige, D. G., Emilion, G. G., Bouloux, P. M., and Harper, J. I. (1994). A clinical and genetic study of X-linked recessive ichthyosis and contiguous gene defects. *Br. J. Dermatology* 131 (5), 622–629. doi:10.1111/j.1365-2133.1994.tb04972.x
- Rijlaarsdam, J., Marinus, H., Frank, C., Vincent, W. V. J., Janine, F., Tiemeier, H., et al. (2017). Prenatal stress exposure, oxytocin receptor gene (OXTR) methylation, and child autistic traits: The moderating role of OXTRrs53576 genotype. *Autism Res.* 10. doi:10.1002/aur.1681
- Sato, J., Denda, M., Nakanishi, J., Nomura, J., and Koyama, J. 1998. Cholesterol sulfate inhibits proteases that are involved in desquamation of stratum corneum." *J. Investigative Dermatology* 111(2): 189–193 .
- Singh, K., Camera, E., Krug, L., Basu, A., Kumar Pandey, R., Munir, S., et al. (2018). JunB defines functional and structural integrity of the epidermo-pilosebaceous unit in the skin. *Nat. Commun.* 9 (1), 3425. doi:10.1038/s41467-018-05726-z
- Sun, W., Ruijuan, X., Wei, H., Junfei, J., Heather, A., Crellin, J. B., et al. (2008). Upregulation of the human alkaline ceramidase 1 and acid ceramidase mediates calcium-induced differentiation of epidermal keratinocytes. *J. Investigative Dermatology* 128 (2), 389–397.
- Tiepolo, L., Zuffardi, O., Fraccaro, M., di Natale, D., Gargantini, L., Müller, C. R., et al. (1980). Assignment by deletion mapping of the steroid sulfatase X-linked ichthyosis locus to Xp223. *Hum. Genet.* 54 (2), 205–206. doi:10.1007/BF00278973
- Wang, K., Ruijuan, X., Yong, Z., GongLouis, C. P.W., et al. (2015). Alkaline ceramidase 3 deficiency results in purkinje cell degeneration and cerebellar ataxia due to dyshomeostasis of sphingolipids in the brain. *PLoS Genet.* 11 (10), e1005591.
- Williams, M. L., Grayson, S., Bonifas, J. N., Epstein, E. H., and Elias, P. M. (1983). "Epidermal cholesterol sulfate and steroid sulfatase activity and recessive X-linked ichthyosis," in *Stratum corneum* (Berlin, Germany: Springer). doi:10.1007/978-3-642-68682-5_10
- Wren, G., Baker, E., Underwood, J., Humby, T., Thompson, A., Kirov, G., et al. (2022). Characterising heart rhythm abnormalities associated with Xp22.31 deletion. *J. Med. Genet.* doi:10.1136/jmg-2022-108862
- Yen, P. H., Allen, E., Marsh, B., Mohandas, T., Wang, N., Taggart, R. T., et al. (1987). Cloning and expression of steroid sulfatase cDNA and the frequent occurrence of deletions in STS deficiency: Implications for X-Y interchange. *Cell* 49 (4), 443–454. doi:10.1016/0092-8674(87)90447-8